

Loss of coherence in dynamical networks: spatial chaos and chimera states

Iryna Omelchenko,^{1,2} Yuri Maistrenko,^{2,3} Philipp Hövel,¹ and Eckehard Schöll¹

¹*Institut für Theoretische Physik, TU Berlin, Hardenbergstraße 36, 10623 Berlin, Germany*

²*Institute of Mathematics, National Academy of Sciences of Ukraine, Tereshchenkivska str. 3, 01601 Kyiv, Ukraine*

³*National Center for Medical and Biotechnical Research,*

National Academy of Sciences of Ukraine, Volodymyrska str.54, 01030 Kyiv, Ukraine

(Dated: June 6, 2018)

We discuss the breakdown of spatial coherence in networks of coupled oscillators with nonlocal interaction. By systematically analyzing the dependence of the spatio-temporal dynamics on the range and strength of coupling, we uncover a dynamical bifurcation scenario for the coherence-incoherence transition which starts with the appearance of narrow layers of incoherence occupying eventually the whole space. Our findings for coupled chaotic and periodic maps as well as for time-continuous Rössler systems reveal that intermediate, partially coherent states represent characteristic spatio-temporal patterns at the transition from coherence to incoherence.

PACS numbers: 05.45.Xt, 05.45.Ra, 89.75.-k

Keywords: dynamical networks, coherence, spatial chaos

Understanding the dynamics on networks is at the heart of modern nonlinear science and has a wide applicability to various fields [1, 2]. Thus, network science is a vibrant, interdisciplinary research area with strong connections to physics. For example, concepts of theoretical physics like the Turing instability, which is a known paradigm of non-equilibrium self-organization in space-continuous systems, have recently been transferred to complex networks [3]. While spatially extended systems show pattern formation mediated by diffusion, i.e., local interactions, a network takes also into account long-range and global interactions yielding more realistic spatial geometries.

Network topologies like all-to-all coupling of, for instance, phase oscillators (Kuramoto model) or chaotic maps (Kaneko model) were intensively studied, and numerous characteristic regimes were found [4–6]. In particular, for globally coupled chaotic maps they range – for decreasing coupling strength – from complete chaotic synchronization via clustering and chaotic itineracy to complete desynchronization. The opposite case, i.e., nearest-neighbor coupling, is known as lattice dynamical systems of time-continuous oscillators, or coupled map lattices if the oscillator dynamics is discrete in time. These kinds of networks arise naturally as discrete approximation of systems with diffusion and have also been thoroughly studied. They can demonstrate rich dynamics such as solitons, kinks, etc. up to fully developed spatio-temporal chaos [6–10].

The case of networks with nonlocal coupling, however, has been much less studied in spite of numerous applications in different fields. Characteristic examples pertain to neuroscience [11, 12], chemical oscillators [13, 14], electrochemical systems [15], and Josephson junctions [16]. A new impulse to study such networks was given, in particular, by the discovery of so-called chimera states [17, 18]. The main peculiarity of these spatio-temporal

patterns is that they have a hybrid spatial structure, partially coherent and partially incoherent, which can develop in networks of identical oscillators without any sign of inhomogeneity.

In this Letter we discuss the transition between coherent and incoherent dynamics in networks of nonlocally coupled oscillators. We start with coupled chaotic maps

$$z_i^{t+1} = f(z_i^t) + \frac{\sigma}{2P} \sum_{j=i-P}^{i+P} [f(z_j^t) - f(z_i^t)], \quad (1)$$

where z_i are real dynamic variables ($i = 1, \dots, N$, $N \gg 1$ and the index i is periodic mod N), t denotes the discrete time, σ is the coupling strength, P specifies the number of neighbors in each direction coupled with the i -th element, and $f(z)$ is a local one-dimensional map. We choose f as the logistic map $f(z) = az(1-z)$ and fix the bifurcation parameter a at the value $a = 3.8$. This choice yields chaotic behavior of the map f with positive Lyapunov exponent $\lambda \approx 0.431$.

Results of direct numerical simulation of the model (1) in the two-parameter plane of the coupling radius $r = P/N$ and coupling strength σ are presented in Fig. 1. This figure reveals the appearance of regions of spatial coherence, shown in shading (color), at an intermediate radius of coupling. Alternatively, if the oscillators are uncoupled ($r = 0$) or coupling is only local ($r = 1/N$) the network displays high-dimensional space-time chaos [6]. In the opposite situation, when the coupling is all-to-all ($r = 0.5$), chaotic synchronization occurs: the oscillators behave identically, but chaotically in time following the dynamics of f [5, 6]. The chaotic synchronization (hatched region $k = 0$) persists for smaller r or σ up to the blowout bifurcation [19] indicated by the curve BB, where the synchronized state loses transverse stability, i.e., the dynamics becomes desynchronized. The spatially homogeneous state represents the simplest example of coherent dynamics.

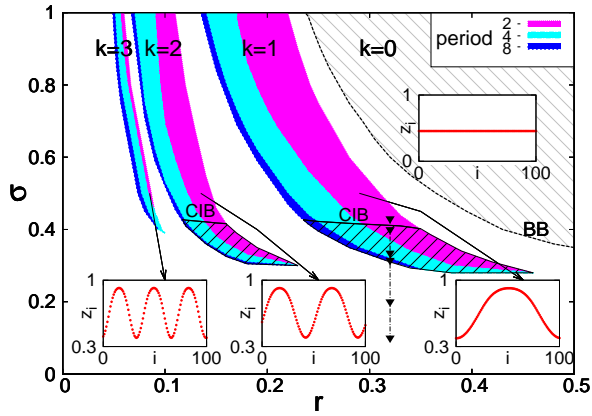


FIG. 1: (Color online) Regions of coherence for system (1) in the (r, σ) parameter plane with wave numbers $k = 1, 2$, and 3. Snapshots of typical coherent states z_i are shown in the insets. Color code inside the regions distinguishes different time-periods of the states. The CIB bifurcation curve separates regions with coherent and incoherent dynamics. In the hatched and shaded (color) regions below CIB two-cluster incoherent states exist. Completely synchronized chaotic states exist in the light hatched region bounded by the blowout bifurcation curve BB. Parameters: $a = 3.8$ and $N = 100$.

In general we call a network state z_i^t , $i = 1, \dots, N$, *coherent* on the ring \mathcal{S}^1 as $N \rightarrow \infty$ if for any point $x \in \mathcal{S}^1$ the limiting value

$$\lim_{N \rightarrow \infty} \lim_{t \rightarrow \infty} \sup_{i, j \in U_\delta^N(x)} |z_i^t - z_j^t| \rightarrow 0, \quad \text{for } \delta \rightarrow 0, \quad (2)$$

where $U_\delta^N(x) = \{j : 0 \leq j \leq N, |j/N - x| < \delta\}$ denotes a network-neighborhood of the point x . If the limit (2) does not vanish for $\delta \rightarrow 0$, at least for one point x , the network state is considered incoherent.

Geometrically, coherence means that in the thermodynamic limit $N \rightarrow \infty$ snapshots of the state z_i^t approach a smooth profile $z(x, t)$ of the spatially continuous version of Eq. (1) given by

$$z^{t+1}(x) = f(z^t(x)) + \frac{\sigma}{2r} \int_{x-r}^{x+r} [f(z^t(y)) - f(z^t(x))] dy. \quad (3)$$

According to the definition given above, a transition from coherence to incoherence occurs when the respective solution profile $z^t(x)$ becomes discontinuous. Note that for networks of phase oscillators the property of coherence and incoherence can also be established with use of the notion of a local order parameter [20, 21].

Regions of coherence and typical shapes of the respective coherent states z_i^t are shown in Fig. 1 as shaded (color) tongues and insets, respectively. A coherent state has a smooth profile characterized by the number of maxima, i.e., the wave number k . Only regions for wave numbers $k = 1, 2$, and 3 are shown. Further decrease

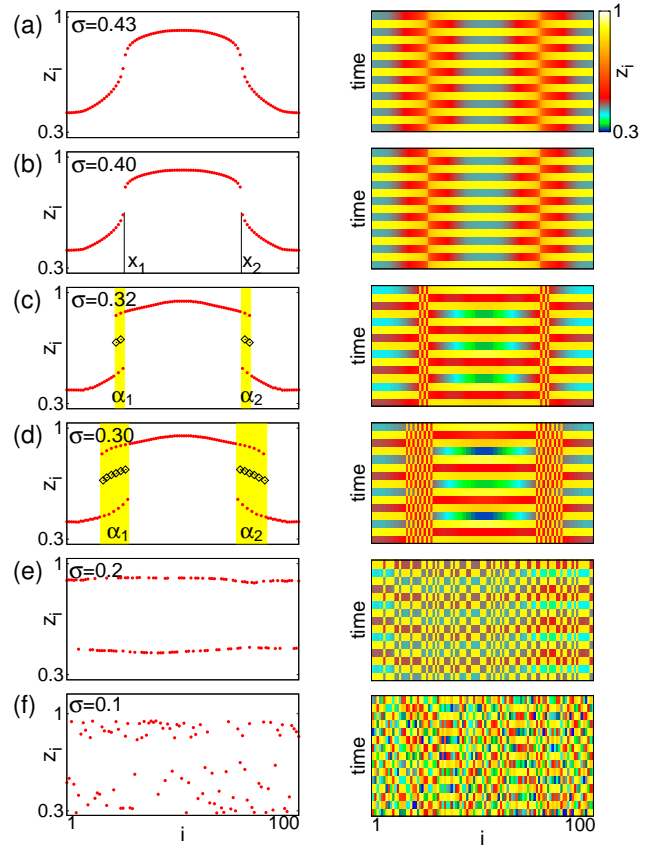


FIG. 2: (Color online) Coherence-incoherence bifurcation for coupled chaotic logistic maps for fixed coupling radius $r = 0.32$ (black triangles in Fig. 1). For each value of the coupling parameter σ (decreasing from top to bottom, $\sigma = 0.43, 0.4, 0.32, 0.3, 0.2$, and 0.1 , respectively) snapshots (left columns) and space-time plots (right columns) are shown. Other parameters as in Fig. 1.

of r yields additional thin higher-order regions following a period-adding cascade $k = 4, 5, \dots$. Inside the regions, the states are coherent in space and periodic in time and undergo a period-doubling cascade of bifurcations in time as r or σ decrease. In the parameter space between the coherence regions the network dynamics remain coherent but not periodic anymore. The states alternate chaotically between the adjacent k -states and thus exhibit chaotic itineracy [6, 22]. The combination of *period-adding* in space and *period-doubling* in time represents a remarkable feature of networks of coupled chaotic oscillators with nonlocal coupling.

A typical scenario of the coherence-incoherence transition is illustrated in Fig. 2(a)-(f), where we fix the coupling radius $r = 0.32$ and decrease the coupling strength σ along the vertical line with triangles in Fig. 1. First, in Fig. 2(a), the solution profile z_i^t is clearly smooth for $\sigma = 0.43$. Thus, the network dynamics is spatially coherent. For smaller σ , the profile z_i^t sharpens up and,

at some value $\sigma \cong 0.40$, loses smoothness in two points x_1 and x_2 as shown in Fig. 2(b). This is a bifurcation point for the coherence-incoherence transition: Beyond this parameter value, the wave-like profile z_i^t splits up into upper and lower branches, and two narrow boundary layers of incoherence are born around the points x_1 and x_2 (shaded yellow stripes α_1 and α_2 in Fig. 2(c)). The incoherence stripes become wider with further decrease of σ (Fig. 2(d)) and, eventually, the dynamics becomes completely incoherent (Figs. 2(e) and (f)).

In our numerical simulations, no coherent states were found below the bifurcation parameter value $\sigma \cong 0.40$. In contrast, numerous hybrid states arise, which are coherent on some intervals of the ring \mathcal{S}^1 and incoherent on the complementary intervals. Typical examples of these partially coherent states are shown in Figs. 2(c) and (d). In the figure, black diamonds mark a threshold within the incoherent regions: If the initial value for a chosen oscillator is located above/below this diamond, with all other oscillators unchanged, it will be attracted by the upper/lower branch. This implies that within the incoherent intervals α_1 and α_2 any combinations of the upper and lower states – so-called *mosaic* [8] or *skeleton* pattern [10] – are admissible and can be realized by appropriate choice of the initial conditions. The coherence-incoherence transition is illustrated by the local order parameter R_i shown in Fig. 3(a) for the snapshots depicted in Fig. 2. It is defined as (cf. Ref. [21])

$$R_i = \lim_{N \rightarrow \infty} \frac{1}{2\delta(N)} \left| \sum_{|j-i| \leq \delta} e^{i\psi_j} \right|, \quad (i = 1, \dots, N) \quad (4)$$

with the phase ψ_j introduced by the mapping $\sin \psi_j = (2z_j - \max_j z_j - \min_j z_j) / (\max_j z_j - \min_j z_j)$ and $\delta/N \rightarrow 0$ for $N \rightarrow \infty$, such that a spatial half-period oscillation is mapped onto the polar angular interval $[-\pi/2, \pi/2]$. R_i is close to unity for the coherent state and decreases in regions of spatial incoherence. For the two cases of complete incoherence (Fig. 2(e),(f)) the local order parameter is much smaller than unity, and fluctuating strongly as a signature of spatial chaos. In case of very small coupling (Fig. 2(f)) the values of z_i are more spread out, and hence R_i varies less strongly between neighboring sites and is on average larger than in Fig. 2(e).

As it is illustrated in the space-time plots of Fig. 2, the temporal dynamics before and after the coherence-incoherence bifurcation remains periodic up to very small coupling, when it is chaotic (Fig. 2(f)). The system's complexity results from the fact that the bifurcation gives rise to a huge multistability of partially coherent states as $N \rightarrow \infty$. Indeed, the number c_N of different partially coherent states born in the bifurcation is $c_N = 2^{dN}$, where d is the fraction of oscillators in the incoherent part ($d = \alpha_1 + \alpha_2$ in the case of two incoherence intervals as in Figs. 2(c) and (d)). It follows that the number of different states grows exponentially fast with N , and the *spatial*

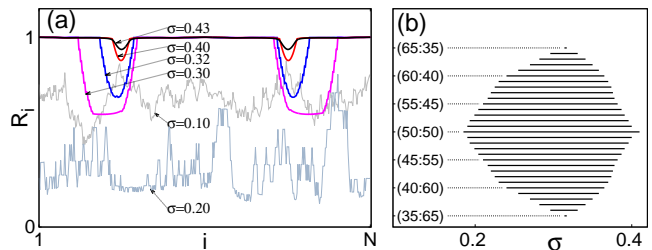


FIG. 3: (Color online) (a): Local order parameter for $r = 0.32$ and different σ as in Fig. 2 (approximated with $\delta = 10$, $N = 400$). (b): Regions of stability for the two-cluster solutions with different asymmetries $(n_1 : n_2)$ as a function of σ for $r = 0.35$. Other parameters as in Fig. 1.

entropy h , which is defined as $h = \lim_{N \rightarrow \infty} (1/N) \ln c_N$, is positive and equals $h = d \ln 2$. Positive spatial entropy means that the system displays *spatial chaos* [8–10], i.e., sensitive dependence on space coordinates. Therefore, the coherence-incoherence bifurcation results instantly in the appearance of spatial chaos that develops first at narrow incoherence intervals and, with decreasing σ , spreads onto the whole ring. Thus a chimera-like state of coexisting coherent and incoherent regions arises as a transitional state in the coherence-incoherence bifurcation scenario. However, in contrast to previously reported chimera states in time-continuous systems [17, 18], the temporal behavior is periodic rather than chaotic, and the complexity arises due to the huge variety of multistable incoherent states corresponding to permutations of the sequence of upper and lower local states. With further decrease of σ , the chimera states disappear giving rise to completely incoherent behavior.

To identify the parameter range for partially coherent states, we define a mosaic of z_i^t as a symbolic sequence of "–" or "+" if the value z_i belongs to the lower or upper branch of the solution profile, respectively. Hence, states as in Fig. 2(b) are given by the mosaic of the form $(\dots - - + + \dots + + - - \dots)$. Therefore, they may be considered as two-cluster states with the ratio of $(n_1 : n_2)$, where n_1 and n_2 are the numbers of "–" and "+" ($n_1 + n_2 = N$), respectively. The ratio $(n_1 : n_2)$ indicates the level of asymmetry of the solution z_i^t , which is important for its stability. Indeed, as it is illustrated in Fig. 3(b) for $r = 0.35$, the symmetric solution (50 : 50) has the widest stability interval $\sigma \in (0.189, 0.41)$. As the asymmetry grows, the stability interval shrinks, and the solution with the mosaic ratio (35 : 65) has the shortest stability interval $\sigma \in (0.314, 0.317)$. Two-cluster solutions with larger asymmetry cannot be stabilized anymore. The states with more complex mosaics, examples of which are presented in Fig. 2(c)-(e), are characterized by more involved mechanisms of stability.

To test if the coherence-incoherence bifurcation is a universal scenario, we have also investigated nonlocally

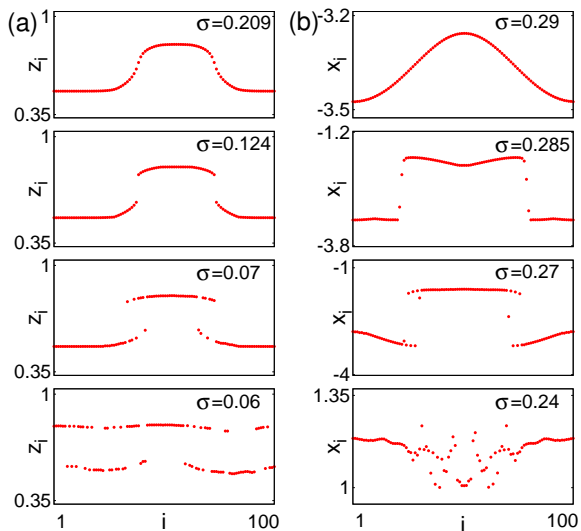


FIG. 4: (Color online) Snapshots with decreasing coupling strength σ : Coherence-incoherence transition for a ring of (a) 100 coupled periodic logistic maps ($a = 3.2$) for a coupling radius $r = 0.1$ and (b) 100 nonlocally coupled Rössler systems ($a = 0.42$, $b = 2$, $c = 4$) with $r = 0.3$.

coupled networks with different local dynamics. Figure 4 shows the coherence-incoherence transition for nonlocally coupled logistic maps (1) in the periodic regime ($a = 3.2$, period 2, Fig. 4(a)) and for nonlocally coupled chaotic Rössler systems

$$\begin{aligned} \dot{x}_i &= -y_i - z_i + \frac{\sigma}{2P} \sum_{j=i-P}^{i+P} (x_j - x_i), \\ \dot{y}_i &= x_i + ay_i, \\ \dot{z}_i &= b + z_i(x_i - c) \end{aligned} \quad (i = 1, \dots, N) \quad (5)$$

(Fig. 4(b)). As it can be seen from the snapshots, both models display a transition from spatial coherence to incoherence, as the coupling strength σ decreases, according to the scenario described above. Since network (5) is time-continuous, the oscillators within the incoherence intervals are not only located at an upper or lower branch of the solution profile, but vary continuously. This gives rise to chaotic temporal dynamics in the incoherent intervals, which resembles known chimera states [17, 18]. We conclude that chaotic chimera states typically arise in the nonlocally coupled Rössler systems, similar to nonlocally coupled Kuramoto-Sakaguchi phase oscillators [18].

In conclusion, we have identified a novel mechanism for the coherence-incoherence transition in networks with nonlocal coupling of variable range. It consists in the appearance of multistable chimera-like states. We have found similar bifurcation scenarios for coupled maps with both chaotic and periodic local dynamics as well as for time-continuous systems. This indicates a common, probably universal phenomenon in networks of very different nature, due to nonlocal coupling.

We thank B. Fiedler, M. Hasler, and M. Wolfrum for illuminating discussions. I. O. acknowledges support from DAAD and DFG (SFB 910). Y. M. acknowledges support and hospitality from TU Berlin.

-
- [1] D. J. Watts and S. H. Strogatz, *Nature* **393**, 440 (1998).
 - [2] C. Song, T. Koren, P. Wang, and A.-L. Barabási, *Nature Physics* **6**, 818 (2010).
 - [3] H. Nakao and A. S. Mikhailov, *Nature Physics* **6**, 544 (2010).
 - [4] Y. Kuramoto, *Chemical Oscillations, Waves, and Turbulence* (Springer, Berlin Heidelberg, 1984), J.A. Acebrón et al. *Rev. Mod. Phys.* **77**, 137 (2005).
 - [5] E. Mosekilde, Y. Maistrenko, and D. Postnov, *Chaotic Synchronization: Applications to Living Systems* (World Scientific, Singapore, 2002).
 - [6] K. Kaneko and I. Tsuda, *Chaos and Beyond, A Constructive Approach with Applications in Life Sciences* (Springer, Berlin, 1996)
 - [7] M. H. Jensen, *Physica Scripta* **T9**, 64 (1985); P. Couillet, C. Elphick, and D. Repaux, *Phys. Rev. Lett.* **58**, 431 (1987); W. Shen, *SIAM J. Appl. Math.* **56**, 1379 (1996); B. Fernandez, B. Luna, and E. Ugalde, *Phys. Rev. E* **80**, 025203(R) (2009).
 - [8] S. N. Chow and J. Mallet-Paret, *IEEE Trans. Circ. Sys.* **42**, 746 (1995).
 - [9] V. Afraimovich, *Some topological properties of lattice dynamical systems* in Dynamics of coupled map lattices and of related spatially extended systems, *Lecture Notes in Phys.* **671**, 153 (Springer, Berlin, 2005).
 - [10] L. P. Nizhnik, I. L. Nizhnik, and M. Hasler, *Int. J. Bif. Chaos* **12**, 261 (2002).
 - [11] D. Battaglia, N. Brunel, and D. Hansel, *Phys. Rev. Lett.* **99**, 238106 (2007).
 - [12] R. Vicente, L. L. Gollo, C. R. Mirasso, I. Fischer, and P. Gordon, *Proc. Natl. Acad. Sci.* **105**, 17157 (2008).
 - [13] C. Beta, M. G. Moula, A. S. Mikhailov, H. H. Rotermund, and G. Ertl, *Phys. Rev. Lett.* **93**, 188302 (2004).
 - [14] A. S. Mikhailov and K. Showalter, *Phys. Rep.* **425**, 79 (2006).
 - [15] N. Mazouz, G. Flätgen, and K. Krischer, *Phys. Rev. E* **55**, 2260 (1997); V. García-Morales and K. Krischer, *Phys. Rev. Lett.* **100**, 054101 (2008).
 - [16] K. Wiesenfeld, P. Colet, and S. H. Strogatz, *Phys. Rev. Lett.* **76**, 404 (1996).
 - [17] Y. Kuramoto and D. Battogtokh, *Nonlin. Phen. in Complex Sys.* **5**, 380 (2002); D. M. Abrams and S. H. Strogatz, *Phys. Rev. Lett.* **93**, 174102 (2004); G. C. Sethia, A. Sen, and F. M. Atay, *Phys. Rev. Lett.* **100**, 144102 (2008); C. R. Laing, *Physica D* **238**, 1569 (2009); E. A. Martens, C. R. Laing, and S. H. Strogatz, *Phys. Rev. Lett.* **104**, 044101 (2010).
 - [18] O. E. Omel'chenko, M. Wolfrum, and Y. L. Maistrenko, *Phys. Rev. E* **81**, 065201 (2010).
 - [19] E. Ott and J. C. Sommerer, *Phys. Lett. A* **188**, 39 (1994).
 - [20] A. S. Pikovsky and M. G. Rosenblum, *Phys. Rev. Lett.* **101**, 264103 (2008).
 - [21] M. Wolfrum, O. E. Omel'chenko, S. Yanchuk, and Y. L. Maistrenko, *Chaos* **21**, 013112 (2011).
 - [22] K. Kaneko and I. Tsuda, *Chaos* **13**, 926 (2003).